

Taylor cone and electro spraying at a free surface of superfluid helium charged from belowP. Moroshkin,^{1,*} P. Leiderer,² Th. B. Möller,² and K. Kono^{1,3,4,†}¹*RIKEN, Center for Emergent Matter Science, 2-1 Hirosawa, Wako, 351-0198 Saitama, Japan*²*Department of Physics, University of Konstanz, Universitätsstrasse 10, 78464 Konstanz, Germany*³*Institute of Physics, National Chiao Tung University, Hsinchu 300, Taiwan*⁴*Institute of Physics, Kazan Federal University, Kremlyovskaya St. 18, 420008 Kazan, Russia*

(Received 23 February 2017; published 19 May 2017)

Electrically charged metallic micro- and nanoparticles are trapped under a free surface of superfluid He in a vertical static electric field. We observe a static deformation of the charged liquid surface in the form of a Taylor cone and the emission of a charged liquid helium jet (electrospray). Our numeric calculations reproduce the static shape of the cone.

DOI: [10.1103/PhysRevE.95.053110](https://doi.org/10.1103/PhysRevE.95.053110)**I. INTRODUCTION**

When an electrically conductive liquid is placed in a strong vertical electric field, its free surface acquires a surface charge that creates an extra pressure directed upwards. As a result, the free surface of the liquid is lifted up and forms a hump or a cone. The phenomenon was studied in detail theoretically and experimentally in the 1960s by G. Taylor [1,2], who derived an analytic solution for the shape of the hump and showed that the vertex angle of the cone is always equal to 98.6° . The structure has since been referred to as a Taylor cone. A similar phenomenon can also be observed in a dielectric liquid or with electric charge carriers injected by some external source. In this case, the electric field inside the liquid is not zero and the problem requires a self-consistent solution that can be done only numerically [3].

When the electric-field strength exceeds some critical value, the cone produces a very sharp jet of charged liquid and/or a spray of droplets shooting upwards. The phenomenon is referred to as electrostreaming or electro spraying. This is a manifestation of a surface hydroelectrodynamic instability that still attracts much attention from researchers [3–7] and is used in many applications.

Cryogenic superfluid helium differs from conventional dielectric liquids in many aspects, most notably by its exceptional purity and vanishing viscosity. The hydroelectrodynamic instability of a charged free surface of superfluid helium had been thoroughly studied theoretically and experimentally [8,9], but in a somewhat different configuration. In those studies, free electrons are attached to the free surface of liquid He from above. They cannot penetrate into the liquid due to a potential barrier of $\approx 1\text{eV}$ [10]. In the external vertical electric field, the electrons create an extra pressure at the liquid-gas interface that may lead to the development of a surface instability. The surface becomes corrugated by so-called multielectron dimples, each containing approximately 10^7 electrons and having a depth of ≈ 0.1 mm and a diameter of ≈ 1 mm [11]. Above some critical electric-field strength, the

electrons push the helium surface farther down and the dimple transforms into a multielectron bubble that moves down into the liquid He bulk [12–14].

Much less is known about the distortions and instability of a liquid He surface caused by the electric charges trapped below the surface. Local lifting of a liquid helium free surface above a submerged negatively charged tip and generation of a jet or a fountain above this tip were reported in [15]. Negatively charged “geysers” of superfluid He have been observed in [16]. A similar effect was also observed in liquid hydrogen [17]. In both experiments [16,17], the liquid was charged with negative ions (electrons) generated by a submerged β -radioactive source.

In the present study, we trap the charges of either polarity under a free surface of superfluid ^4He , in a vertical static electric field. We observe static surface deformations and superfluid He jets or geysers similar to those reported in [16]. A light-scattering technique is applied to investigate the species trapped under the surface.

II. EXPERIMENTAL SETUP

The experimental setup is similar to that described in our recent publication [18]. The sample cell is installed in the optical helium-bath cryostat shown in Fig. 1(a). The temperature is adjusted in the range of $T = 1.35\text{--}2.17$ K by pumping on the liquid He in the bath. The sample cell is immersed in the He bath and is filled with condensing He gas from a high-pressure gas cylinder. The cell and the cryostat have four side windows and a window in the bottom. The windows have a clear aperture of 20 mm.

The liquid He in the cell is doped with neutral and electrically charged particles by laser ablation from a metal Ba target positioned in the liquid. The ablation is done either with a pulsed frequency-doubled Nd:YAG laser ($\lambda = 532$ nm) or with a frequency-tripled pulsed diode-pumped solid-state laser ($\lambda = 355$ nm). The Nd:YAG laser produces nanosecond pulses with a repetition rate of up to 10 Hz and a pulse energy of 0.1 to 10 mJ. The diode-pumped solid-state laser has the higher maximum repetition rate of 100 Hz with a pulse energy of $70\ \mu\text{J}$. The ablation laser beam enters the cell via one of the side windows and hits the vertical target surface. Outside the cryostat, the laser beam is expanded to a diameter of ≈ 3 cm and then focused by a lens with a focal distance of 10 cm,

*petr.moroshkin@riken.jp

†http://www.riken.jp/en/research/labs/cems/qtm_inf_electron/qtm_condens_phases/

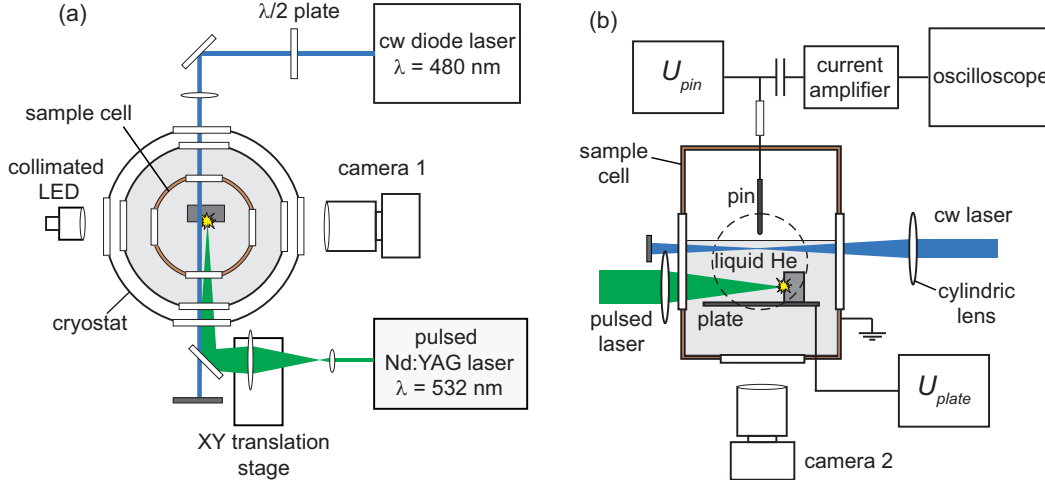


FIG. 1. Experimental setup. Left: Top view of the cryostat and optical setup. Right: Vertical cut through the sample cell and electric current measurement circuit.

positioned in front of the cryostat window. In order to prevent the hole-drilling effect, the focus of the laser beam is moved continuously along the target surface by translating the lens in the plane orthogonal to the optical axis.

The target has horizontal dimensions of 4×6 mm and a height of 5 mm. It is positioned in the lower part of the cell, on top of a horizontal flat electrode, as shown in Fig. 1(b). This electrode is made either of copper or of a 0.7-mm-thick glass with a conductive transparent film on the upper surface. The copper electrode has the shape of a disk, 4 cm in diameter. The glass electrode has a rectangular shape, 35×25 mm. It allows us to monitor the interior of the cell and, in particular, the liquid He surface via the window at the bottom. On the vertical axis of the cell, a vertical pin electrode is installed. The pin is 1.6 mm in diameter and has a rounded tip pointing down. The upper end of the pin is connected to a high-voltage feedthrough in the ceiling of the cell. The tip is positioned 7–15 mm above the upper edge of the ablation target, 12–20 mm above the horizontal electrode.

The body of the sample cell is electrically grounded. Both the horizontal plate and the pin are connected to high-voltage power supplies of opposite polarities. During the experiment, their electric potentials, U_{plate} and U_{pin} , are set independently in the range of ± 2000 V. The ablation target has the same potential as the plate.

The ablation target is positioned in front of the lower part of the window, while the tip of the pin can be seen in the upper part. The cell is filled with liquid He up to a certain height, such that the free surface of the liquid is approximately 1 mm below the tip and can be clearly seen through the side windows. The free surface and the space between the surface and the plate are monitored with a digital video camera, shown in Fig. 1(a), oriented either horizontally or at an angle of $-15^\circ \leq \theta \leq +15^\circ$ with respect to the horizon. In the experiment with the transparent horizontal electrode, the camera is installed at the bottom window of the cryostat, as shown in Fig. 1(b). The camera is equipped with a macrolens that has a magnification equal to 1 and a focal distance of 12 cm. The camera is operated at a frame rate of 100–5300 fps and allows us to study the waves and the

static deformations at the free surface. The cell is illuminated either by a white halogen lamp or by a collimated blue LED.

In order to visualize the injected metallic particles, we use scattered light from the beam of a cw frequency-doubled diode laser with a wavelength $\lambda = 480$ nm. It is aligned horizontally, orthogonal to the optical axis of the camera. The beam is expanded to a diameter of 6 mm and then focused in the middle of the cell by a cylindrical lens with a focal distance of 15 cm. The direction of the linear polarization of the laser is adjusted by a $\lambda/2$ plate in order to maximize the light-scattering efficiency.

We measure the electric current arriving at the pin electrode due to the charge escaping from the liquid He trap. The current measurement electronics is connected to the pin via a high-voltage capacitor, $C = 1$ nF, and a 1-M Ω resistor, as shown in Fig. 1(b).

III. SIMULATIONS

An essential quantity for the understanding of the Taylor cone phenomena in our measurements is the total number of charges (which in a particular run is constant, as long as no breakthrough occurs) and their distribution across the surface. This information can be derived from the charge-induced deformation of the surface, but not in a simple analytical manner. We have therefore carried out finite-element simulations in which the surface displacement $u(r)$ and the corresponding charge density distribution $\rho_{\text{el}}(r)$ were determined self-consistently. The commercial software package COMSOL Multiphysics was used for this purpose. A schematic of the simulated domain is shown in Fig. 2. The walls of the cylindrical sample cell (diameter, 54 mm; height, 70 mm) are on ground potential, $U = 0$, the potential applied to the (bottom) plate electrode is U_{plate} , and the (top) pin electrode is at U_{pin} . The diameters of the bottom plate and the pin are 40 and 1.6 mm, respectively, the distance between the plate and the tip of the pin is 20 mm, and the distance between the pin and the (undeformed) helium surface is 1.3 mm. The liquid surface is sketched with a hillock below the pin due to the electrostatic force acting on the charge pool (in red). The electrostatic potential in the charge pool is

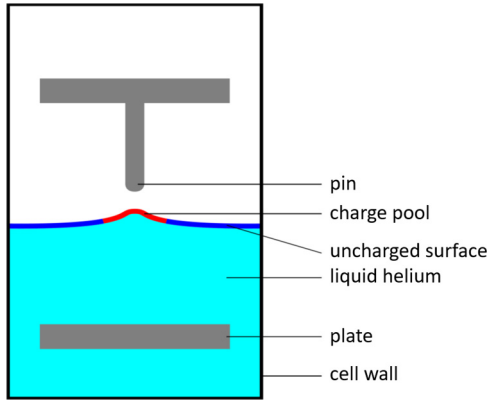


FIG. 2. Schematic of the sample cell with top and bottom electrodes and the charged helium surface.

assumed to be constant but not fixed. The simulations result in a charge distribution with a sharp circular edge, the surface outside (drawn in blue) is uncharged. The dielectric constant of the liquid helium is $\epsilon_r = 1.059$, for the vapor phase we use $\epsilon_r = 1$. Only static phenomena are considered here.

The potential difference $U_{\text{pin}} - U_{\text{plate}}$ applied between tip and bottom plate was studied in the simulations up to 2000 V. Under the influence of these potentials the charges arrange themselves in such a way across the helium surface that there is a central charged pool, surrounded by an area with no charge. The calculation of the electrostatic potential in the sample cell is based on $\text{div}(\mathbf{D}) = \rho_{\text{el}}$ and $\mathbf{E} = -\text{grad}(U)$, where \mathbf{D} is the electric displacement and \mathbf{E} is the electric field. In the charge pool the liquid surface is an equipotential surface; the component of the electric field parallel to the surface therefore has to vanish in this region in the static case.

The surface displacement $u(r)$ follows from

$$-\gamma \nabla^2(u) + g\rho u = \rho_{\text{el}} E_z, \quad (1)$$

where we have used the approximation that the radius of curvature of the surface is much larger than u . Here $\gamma = 3 \times 10^{-4}$ N/m is the surface tension of liquid helium around $T = 2$ K, $\rho = 145$ kg/m³ is the helium density in this temperature range, and g is the acceleration due to gravity. E_z is the z component of the electric field derived from electric potential calculations.

IV. RESULTS

A. Taylor cone

Laser ablation of metals in liquid He produces a large amount of electrically charged species of both polarities. These can be metal ions, free electrons, charged clusters, nanoparticles, and micro-particles [19–22]. In a vertical static electric field, depending on the field polarity, either positive or negative charge carriers are driven upwards and accumulate under the free surface of the liquid. Due to the radial (horizontal) component of the electric field created by the pin and plate electrodes, the charges concentrate on the axis of the cell, under the tip of the upper electrode. The electrostatic force creates an extra pressure on the liquid surface directed upwards that has a maximum right under the tip. We therefore

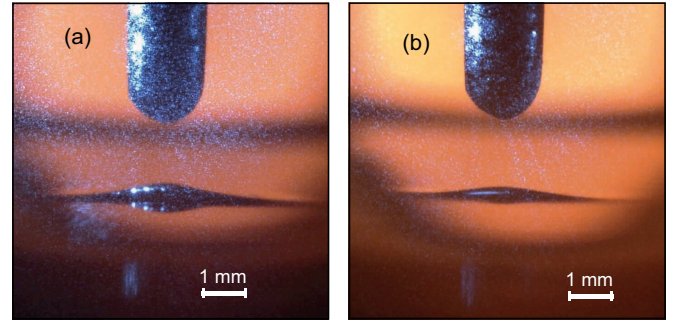


FIG. 3. A static deformation of the free surface of superfluid He (Taylor cone) due to the trapped charge in a static electric field. (a) Negative charge trapped; (b) positive charge trapped. $T = 2.1$ K.

observe a local lifting of the free surface of superfluid He under the tip, as shown in Fig. 3. It has a height of 0.1–0.3 mm and a diameter of ≈ 3 –5 mm at the base, or ≈ 1 –2 mm at half-height. Such a pronounced surface deformation in the form of a hillock (Taylor cone) can be observed, with the potential difference between the plate and the pin of the order of 500 V or more. No static deformation could be observed in the absence of injected charges even at the highest applied field strength. This is not surprising, because the electric-field-induced deformation of the helium surface under these conditions is expected to be just a few micrometers, which is below the resolution of our experiment. A sufficient amount of charge is typically produced by one to five successive ablation laser pulses with an energy of 70–300 μJ per pulse, fired at a rate of 1 Hz. Increasing the laser pulse energy or the repetition rate leads to the generation of surface waves in liquid He and to the loss of the trapped charge and destruction of the hillock.

Very similar Taylor cones have been obtained at either polarity of the applied voltage. This observation is illustrated by the two photos in Figs. 3(a) and 3(b), which show the deformations produced by trapping negative and positive charges, respectively. In both pictures, the surface is illuminated by a halogen lamp shining from the opposite side of the cryostat and by a cw blue laser beam that crosses the cell from left to right. The latter is scattered by the particles trapped under the surface.

Increasing the applied electric field leads to an increase in the height of the cone. The effect is illustrated in Fig. 4, where the observed cone height is plotted versus the applied voltage. In that experiment, the potential of the pin was fixed at $U_{\text{pin}} = -400$ V and the potential of the bottom electrode (copper disk) was increased in steps of 100 V from $U_{\text{plate}} = 0$ to $U_{\text{plate}} = +1300$ V. At a high voltage, the dependence becomes nonmonotonic. There are sudden jumps down that occur at some values of $U_{\text{plate}} - U_{\text{pin}}$ that are poorly reproducible for different Taylor cones created under the same conditions. Each jump corresponds to the escape of some amount of charge from the liquid.

B. Charge escape

In Fig. 5 we show a sequence of frames from a video recording taken during one charge escape event. The video was recorded at a frame rate of 5334 fps. Thus every frame

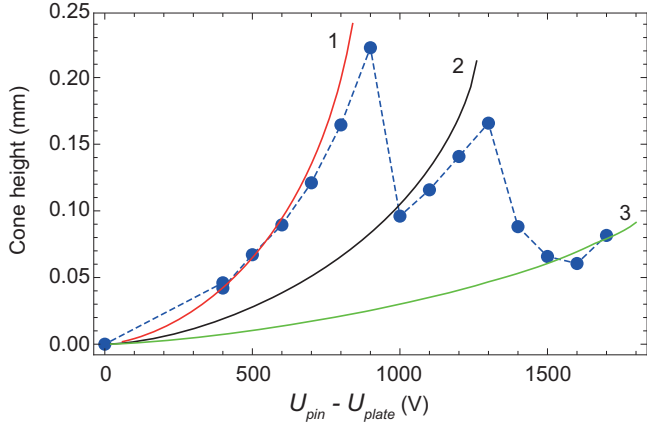


FIG. 4. Height of the Taylor cone as a function of the plate-to-pin voltage difference. Experimental data: circles connected by dashed line. U_{pin} is fixed at -400 V and U_{plate} increased in steps of 100 V; $T = 2.1$ K. Calculations (see Sec. V A): solid curve 1 (red), cone charge $3.2 \times 10^8 e$; curve 2 (black), cone charge $3.2 \times 10^7 e$; curve 3 (green), $4 \times 10^6 e$.

corresponds to a 0.19 -ms time interval. Initially, the cone has a rounded top [Fig. 5(a)]. Close to the breakdown, a cusp appears at the very top of the cone [Fig. 5(b)]. A narrow jet of liquid He is then emitted from the cusp upwards and hits the tip of the upper electrode [Figs. 5(c) and 5(d)]. The jet can be seen during ≈ 3 ms and has a diameter of ≈ 20 – $30 \mu\text{m}$. After the ejection of the charge, the surface of the liquid under the tip jumps down, below the level of the undisturbed liquid [Figs. 5(e) and 5(f)].

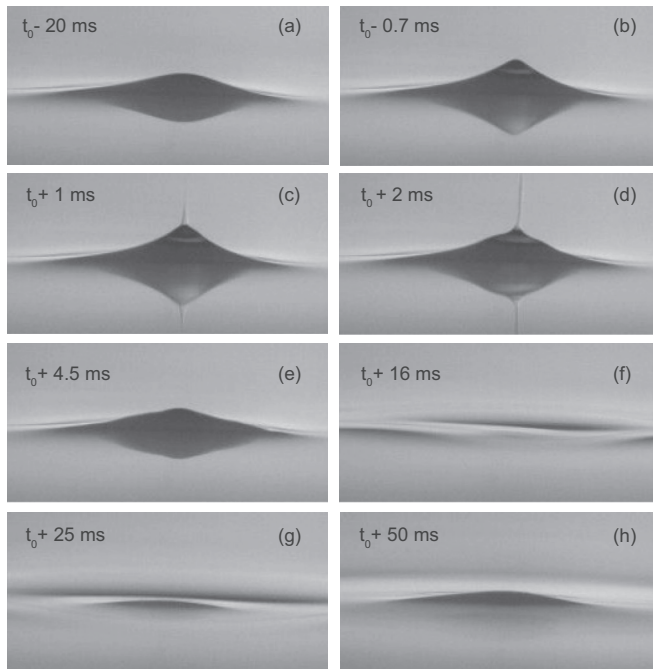


FIG. 5. Frames of a fast video recording capturing the process of the charge escape from the Taylor cone. $U_{pin} = -390$ V, $U_{plate} \approx +900$ V (ramp from $+800$ to $+1800$ V), $T = 2.1$ K, single-frame exposure time ≈ 0.19 ms; time $t = t_0$ corresponds to the beginning of the jet emission. Frame size, 4.6×2.5 mm.

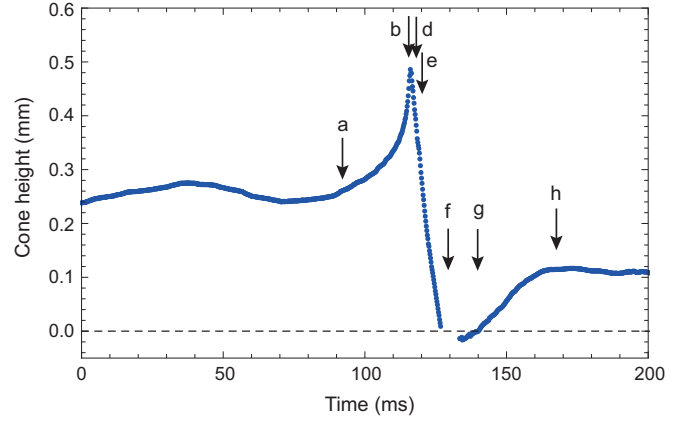


FIG. 6. Time dependence of the height of the Taylor cone corresponding to the video recording in Fig. 5. Every data point corresponds to one frame in the video. $U_{pin} = -390$ V, $U_{plate} \approx +900$ V (ramp from $+800$ to $+1800$ V), $T = 2.1$ K, single-frame exposure time ≈ 0.19 ms. Vertical arrows mark the moments corresponding to the frames shown in Fig. 5. The dashed horizontal line shows the level of the undisturbed liquid.

This generates a circular surface wave running from the center to the periphery that decays within some 50 – 100 ms [Figs. 5(f) and 5(g)]. At the same time a residual smaller cone emerges in the center [Figs. 5(g) and 5(h)]. In each frame in Fig. 5, the corresponding time is indicated. $t = t_0$ corresponds to the moment when the jet is first observed. A slow-motion movie of a typical charge escape event is provided in the Supplemental Material [23].

The apex angle θ of a static cone varies over a broad range and decreases with increasing cone height. In order to determine the angle, the cone profile in several most typical images has been digitized and fitted by fourth-order polynomials. The slope of each side of the cone was then obtained by computing the derivative of the corresponding polynomial. The cone angle is calculated as the difference between the slopes on both sides at the same height. The cone that is far from the breakdown by jet emission typically has a rounded top. In this case we take the slopes in the range where the cone sides are approximately straight: between 50% and 80% of the cone height. The slope of the cone sides in this range is largest. It decreases towards the base of the cone and towards the top. The vertex angle determined in this way is typically $\theta \approx 150^\circ \pm 10^\circ$. The cone that is close to a breakdown is higher and has a sharp cusp at the top [Figs. 5(b) and 5(c)]. The slope on each side increases monotonically from the base of the cone towards the top. The apex angle measured at the very top of the cone approaches $\theta \approx 100^\circ$, which is very close to the value predicted by Taylor, $\theta = 98.6^\circ$.

The time dependence of the height of the cone during the charge escape process is shown in Fig. 6. Every data point in the figure corresponds to one frame of the video recording. The frames shown in Fig. 5 are marked with vertical arrows.

In order to find the amount of electric charge trapped inside the Taylor cone, we measure the electric current pulses on the pin electrode arising due to the charge escape events. The experimental setup is shown in Fig. 1(b) and the time chart

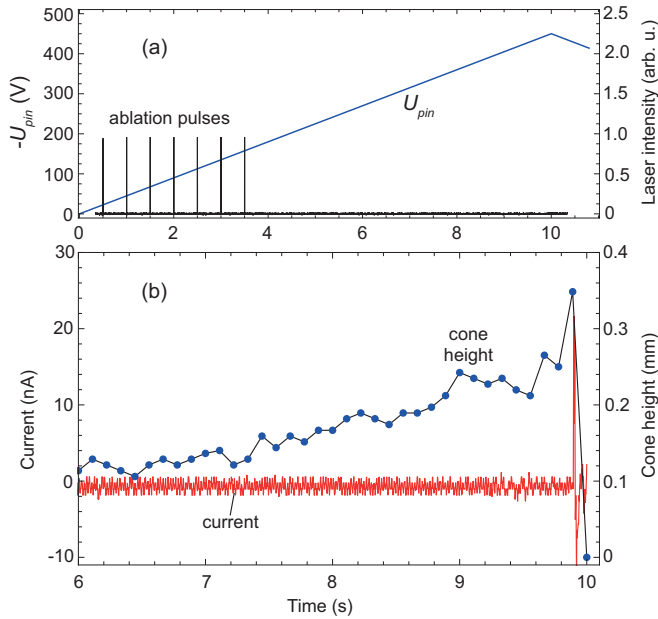


FIG. 7. (a) Voltage ramp applied to the pin electrode U_{pin} and the ablation laser pulses ($\lambda = 532$ nm; pulse energy, $200 \mu\text{J}$). (b) Electric current due to the charge escape and the height of the observed Taylor cone. $U_{\text{plate}}, +890$ V; $T = 2.11$ K.

of the experiment is plotted in Fig. 7(a). The video recording of the Taylor cone at 100 fps is taken synchronously with the current measurement and the observed cone height vs time is plotted in Fig. 7(b). We keep the potential of the plate constant, $U_{\text{plate}} = +890$ V, and apply a periodic voltage ramp at the pin electrode. As shown in Fig. 7(a), U_{pin} is increased linearly from 0 to -450 V in 10 s and then decreased at the same rate. Eight ablation laser pulses ($\lambda = 532$ nm, $200 \mu\text{J}$ per pulse) are fired at 0.5-s intervals at the beginning of the voltage ramp. A typical recording of the current is shown in Fig. 7(b). During the voltage ramp, the capacitor connected to the pin is charged and discharged with a constant current of ± 50 nA. This dc offset is subtracted from the signal shown in 7(b). At the end of the ablation sequence, U_{pin} approaches -200 V and the Taylor cone has a height of ≈ 0.1 mm [Fig. 7(b)]. It increases with the applied voltage and reaches ≈ 0.3 mm. Close to the end of the voltage ramp, at $U_{\text{pin}} \approx -440$ V, the cone emits a helium jet and the surface of the liquid jumps down. At this moment, a short pulse of electric current is registered. In some recordings, the Taylor cone grows up and jumps down several times within the same voltage ramp. Each of these events is accompanied by an electric current pulse.

At $U_{\text{pin}} \approx -500$ to -600 V, typically after a cone breakdown, a corona discharge is ignited at the tip of the pin electrode. The onset of corona discharge manifests itself as a greatly increased noise in the current recording (see Fig. 8). It is also seen in the video recordings of the process. At this polarity of the applied voltage, the corona discharge produces a large amount of free electrons that accelerate towards the plate electrode and impinge on the liquid He surface. The remaining Taylor cone is immediately destroyed, probably because of the neutralization of the trapped positive charge by the electrons. A dimple is formed in the place of the cone and remains there

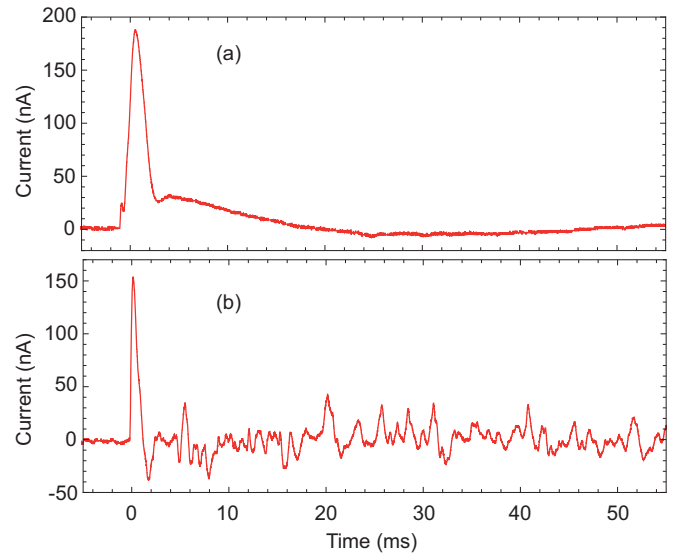


FIG. 8. Electric current pulse associated with the Taylor cone breakdown. (a) No corona discharge, $U_{\text{pin}} = -370$ V, $U_{\text{plate}} = +600$ V; (b) corona discharge starts after the cone breakdown, $U_{\text{pin}} = -400$ V, $U_{\text{plate}} = +600$ V, $T = 2.11$ K.

until the corona discharge goes off at some lower value of the pin potential. The whole cycle of the Taylor cone growth and breakdown and the onset of the corona discharge can be repeated many times.

A typical current pulse associated with the Taylor cone breakdown is shown in Fig. 8(a), and that followed by a corona discharge is shown in Fig. 8(b). The pulse amplitude is about 100–200 nA and a typical pulse width is about 1–2 ms, which is very close to the observed lifetime of the liquid He jet. Each jet thus transports a charge of $\sim 10^{-10}$ C, which can be used as an estimate of the amount of charge that is needed to create a Taylor cone in superfluid He.

C. Light scattering by trapped particles

It has been demonstrated in our preliminary experiments [22] that the laser ablation of a Ba target in liquid He produces a large amount of Ba^+ ions, which could be observed spectroscopically in the ablation plume. It was therefore expected that some amount of Ba^+ ions may be trapped within the Taylor cone at the surface of liquid He. The wavelength of the cw laser used for the light-scattering studies in the present experiment ($\lambda = 480$ nm) was chosen such that it corresponds to the $6^2S_{1/2} \rightarrow 6^2P_{1/2}$ transition of Ba^+ in liquid He [24,25]. The laser-excited ions are expected to emit fluorescence at $\lambda = 492$ nm [24,25]. The wavelength for the emission is different from that for the absorption due to the Ba^+ -He interaction, which makes it easily distinguishable from the laser light scattered by the liquid He surface and by any other ablation products. The spectrum of light scattered by the Taylor cone at right angle was analyzed by a grating spectrometer (not shown in Fig. 1). The observed spectra demonstrate no features that could be assigned to Ba^+ or any other atomic or molecular species. The scattered radiation has the same wavelength as the incident laser beam and therefore has to be assigned to some larger metallic particles. Our estimates [18] suggest that

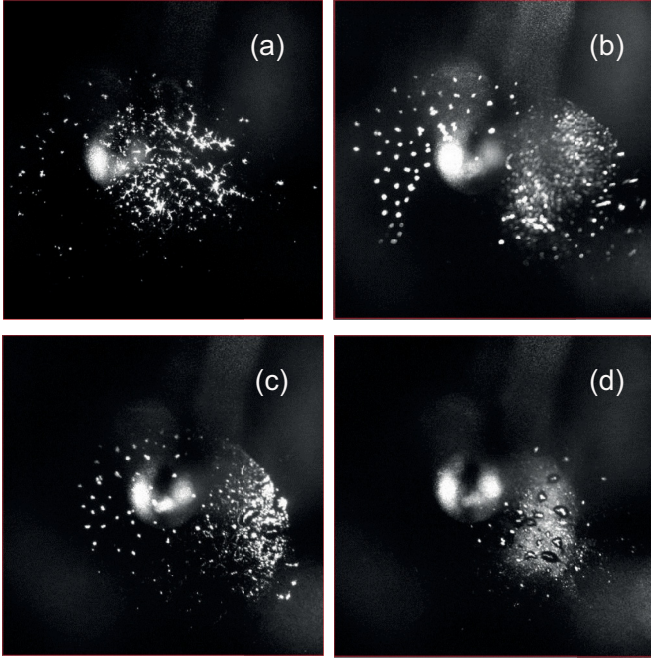


FIG. 9. Frames of a fast video recording showing positively charged nano- and microparticles trapped under the surface of a Taylor cone. View from the bottom; each picture covers the area of 7.5×7.5 mm. $U_{\text{pin}} = -800$ V, $U_{\text{plate}} = +1000$ V, $T = 2.1$ K. (a) Exposure time, 2 ms; cw laser power, 200 mW; (b–d) exposure time, 10 ms; cw laser power, 55 mW.

a spherical Ba particle with a radius larger than 50 nm may scatter a sufficient amount of laser radiation at 480 nm to be detected by the video camera used in the present experiment.

In Fig. 9 we show typical images of the positively charged particles trapped under the surface of a Taylor cone at $U_{\text{pin}} = -800$ V, $U_{\text{plate}} = +1000$ V. The pictures are taken via the window in the bottom of the sample cell, and the particles are illuminated by the cw blue laser. Each picture covers an area of 7.5×7.5 mm, with the tip of the pin electrode shown as a round bright object approximately in the center. In these images, the particles form a quasistatic array determined by the attraction towards the tip and the mutual repulsion of the particles. The real size of the particles, most likely, is not resolved. Some particles are positioned at equal distances and seem to form a quasiperiodic lattice. However, there is no global periodicity over the whole particle cloud and the interparticle distances within the cloud vary quite strongly.

Besides pointlike particles, we observe two types of larger structures: “snowflakes” and a layer of small particles which are too densely packed to be resolved individually with our optical setup. Several large snowflakes with many branches are shown in Fig. 9(a). They strongly resemble the nanowire networks observed at the free surface of superfluid He in experiments with the ablation target positioned above the liquid [18]. Similar nanowire networks have also been created by laser ablation in bulk superfluid He [26,27] and in He nanodroplets doped with metal atoms and clusters [28–30]. The structures of the second kind are visible on the right side of Fig. 9(c) and in Fig. 9(d). The structure can be described as a film or a continuous layer of very fine particles with voids.

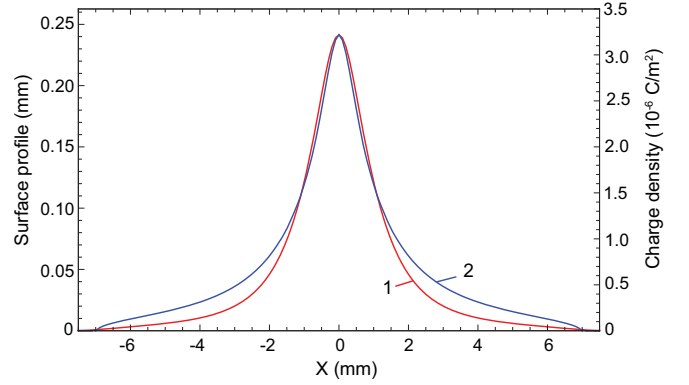


FIG. 10. Surface profile (curve 1) and charge density (curve 2), obtained from a simulation for an applied voltage difference between tip and bottom plate of 1300 V and a total of 1.75×10^8 elementary charges (2.8×10^{-11} C) trapped under the surface.

In the center of each void, one larger particle, or snowflake, is positioned. Apparently, the local electric field created by such relatively large particles is sufficiently strong to push the smaller particles away, resulting in a void or a cavity in the film. Our fast video recordings show fluctuations of the particles and these larger structures, as well as a relatively slow drift, or rotation, of the whole cloud. A reduction in the electric-field strength leads to some spreading of the cloud and, eventually, to the loss of the particles from the trap.

V. DISCUSSION

A. Static cone shape and charge distribution

A perfect dielectric with zero conductivity may produce a Taylor cone only if its dielectric permittivity exceeds a certain threshold, $\epsilon_r \geq 17.6$ [31,32]. The vertex angle in that case is smaller than the Taylor angle of 98.6 characteristic of conductive liquids. However, most observations of Taylor cones in dielectric liquids so far have been made with so-called leaky dielectrics possessing a finite conductivity due to dissolved impurities.

Pure liquid He is a nearly perfect dielectric with an exceptionally small dielectric permittivity, $\epsilon_r = 1.059$, and vanishing conductivity. It contains practically no impurities since at this low temperature all impurity particles become frozen at the walls of the container. Charge carriers created due to cosmic rays and background radiation passing through the liquid mostly recombine immediately after the ionization event. The resulting rate at which electrons become dissolved in superfluid He was measured in [33] to be about 0.04 s^{-1} within a sample volume of the order of 1 cm^3 . They typically leave the sample volume due to diffusion or thermally driven liquid flow (counterflow) at a higher rate. It is thus impossible to create a Taylor cone in liquid He without the injection of charge carriers from outside. In our experiment, the charge is injected by means of laser ablation. Unlike other studies, the amount of charge in our experiment is an independent parameter that, together with the external-field strength, defines the cone size and shape.

An example of our numerical results is presented in Fig. 10. It shows the surface deformation and the corresponding charge

distribution, calculated by means of the simulations mentioned in Sec. III. The input parameters here were a total number of elementary charges of 1.75×10^8 and a potential difference $U_{\text{pin}} - U_{\text{plate}} = 1300$ V applied between the tip and the bottom plate. The cell wall potential was set to the value of the bottom plate in this case. The profile of the Taylor cone in Fig. 10 has an FWHM (full width at half-maximum) of 2.0 mm and a height of 0.24 mm. The charge density reaches a value of 2×10^{13} e/m² in the center of the cone, and the FWHM is the same as that of the cone. For distances >7.0 mm from the center the charge density at the surface is identical to 0, while there is still a small elongation of the surface in this range. The charge distribution in the central part, however, follows the cone profile relatively closely.

In order to compare the simulation results with our measurements, we have plotted in Fig. 4 the calculated height of the Taylor cone as a function of the applied potential difference between the tip and the bottom plate for three different total charges, together with the experimental data. The solid curves representing the simulations display a quite good agreement with the experimental data points for the chosen charge values. Not only is the functional dependence similar, but also the maximum cone heights that are reached experimentally and in the simulations have comparable values: <0.3 mm in both cases. Beyond this height the simulations no longer converge, and in the experiments the already mentioned breakthrough of the surface charge is observed. The total charge which leaves the surface in such an event was found to be of the order of 10^{-10} C, again in agreement with the simulations. One has to keep in mind, though, that the simulations very close to the instability are not expected to be quantitatively correct because of the approximation that the radius of curvature of the deformed liquid surface has to be much larger than the cone height.

The knowledge that in the Taylor cone up to some 10^8 elementary charges are accumulated in an area of a few square millimeters has implications for another experiment which motivated some of the investigations reported here: Ba⁺ ions underneath the surface of liquid helium could be an interesting test object, e.g., in the search for Majorana quasiparticles at the surface of superfluid ³He-B [22]. The Ba⁺ ions are to be detected by spectroscopic means, and the total amount collected in a Taylor cone should be more than enough for a spectroscopic detection. In spite of this expectation, preliminary experiments have not yielded any signal so far. This suggests that, using the laser ablation technique, the majority of the charges in the Taylor cone are species different from Ba⁺, for example, charged nanoparticles and clusters thereof.

One may wonder whether the presence of a significant amount of charge carriers can modify the properties of liquid He. In particular, it is well known that the interaction with impurities, especially with positive ions, can cause localization of He atoms and thus suppress the superfluidity in the vicinity of the impurity particle. The characteristic distance at which neutral He atoms can be attracted and localized near the charged particles is expected to be of the order of 1 nm. This is similar to the radius of a cluster formed around a single He⁺ ion embedded in liquid He, a so-called “snowball” [34]. Assuming all trapped charge carriers to be atomic ions, a charge density

of the order of 10^{13} e per square meter corresponds to a mean interparticle distance that is larger than 200 nm. Each trapped nano- or microparticle, most likely, carries significantly more than one elementary charge and the mean distance between them is even larger. The ensemble of charge carriers trapped under the surface of the cone is thus rather dilute. So far all our observations are consistent with the model assuming that the trapped charge does not affect the macroscopic properties of the liquid.

B. Electrospaying

The dynamics of the Taylor cone breakdown has been investigated theoretically in [3] and [35]. In a perfectly conducting liquid the breakdown is governed by a mechanism known as conic cusping singularity. The fluid is accelerated towards the tip of the cone in a nearly spherically symmetric flow. The redistribution of charge towards the tip is compensated by an instantaneous supply of extra charge due to the infinitely high electric conductivity. As a result, the electrostatic pressure always balances the capillary pressure and the cone preserves its shape. Only the tip of the cone becomes sharper and emits a narrow jet of charged liquid. In a leaky dielectric, the mechanism of the breakdown is different. The charge is transported primarily by the liquid flow along the surface towards the tip. Because of the low conductivity of the liquid, the redistribution of charge along the surface is not compensated rapidly enough. The balance of electrostatic and capillary pressure is not maintained and the upper part of the cone becomes sharper. The cone acquires a characteristic concave shape.

In order to compare our observations with the numeric results in [3], we estimate the typical values of parameters governing the process of electrohydrodynamic tip streaming: Ohnesorge number $\text{Oh} = \eta / \sqrt{\rho\gamma L_0}$, electric bond number $\Gamma = \varepsilon_0(U_{\text{pin}} - U_{\text{plate}})^2 / 2\gamma L_0$, capillary time scale $t_c = \sqrt{\rho L_0^3 / \gamma}$, and electric charge relaxation time $t_e = \varepsilon_0 \varepsilon_r / \sigma$. Here, ρ , η , γ , and σ are the density, viscosity, surface tension coefficient, and electric conductivity of the liquid, respectively. L_0 is the depth of the liquid. At the temperature of our experiment $\rho = 145$ kg/m³, $\eta \approx 10^{-6}$ Pa · s, and $\gamma \approx 3 \times 10^{-4}$ N/m. For $L_0 \approx 1$ cm and $U_{\text{pin}} - U_{\text{plate}} \approx 1000$ V we thus obtain $\text{Oh} \approx 5 \times 10^{-3}$, $\Gamma \approx 1.5$, and $t_c \approx 7$ ms.

The value of the Ohnesorge number provides a measure of the relative strength of viscous forces with respect to the surface tension and inertia. As one may expect, in superfluid He the dynamics is determined by the effect of the surface tension and not by the viscosity. This situation is not unique for superfluid He. In most experiments on classical dielectric liquids, Oh lies in the range of 3×10^{-3} to 10^{-1} . The capillary time for the classical liquids typically lies in the range of 100 μ s to 10 ms. The value of t_c realized in the present work is close to the upper boundary of this range. It should be noted that in most cases the characteristic length scale is given not by the depth of the liquid but, rather, by the diameter of the nozzle, on which a conical meniscus is formed. It leads to a slightly different definition of both t_c and Oh.

It is more difficult to estimate the charge relaxation time. The natural electric conductivity of liquid He is orders of magnitude lower than that of the leaky dielectrics studied up

TABLE I. Parameters of the liquid He jets observed in the present work and in [16].

	Present work	Ref. [16]
T (K)	2.1	1.2
Jet diameter (μm)	20	10
τ_{jet} (ms)	3	1
E (V/cm)	900	1900
Charge (C)	10^{-10}	10^{-11}
τ_{current} (ms)	1–2	1

to date. However, when doped with charge carriers liquid He may conduct a significant electric current. Doping of liquid He with a large amount of positive ions was demonstrated in our recent experiment [36]. In an external electric field of the order of 400 V/cm, the space-charge-limited stationary current density can reach 10^{-8} A/cm², which corresponds to an ion density of $\simeq 10^8$ cm⁻³. One thus can introduce an effective conductivity $\sigma_{\text{eff}} \lesssim 10^{-9}$ S/m that will depend on the injected ion density. It is also expected that σ_{eff} will strongly depend on the liquid helium temperature due to the strong temperature dependence of the ionic mobilities [37,38].

The resulting charge relaxation time is $t_e \gtrsim 10$ ms. It is of the same order as, or larger than, the capillary time t_c . Indeed, the cone breakdown process and the jet emission occur within 1–2 ms, significantly faster than t_e . The scenario of the tip streaming proposed in [3] for leaky dielectrics thus applies to superfluid He as well. This explains the concave shape of the cone during the charge escape process. Our results are obtained at lower values of Bond and Ohnesorge numbers than those investigated in [3]. However, the observed tip streaming looks quite similar. So far we have not identified any specific feature that can be attributed to the fact that helium is superfluid.

In Table I we compare the parameters of the helium jets observed in the present experiment with those of the “geysers” reported in [16]. They are very similar in most aspects, although only negatively charged liquid He was investigated in [16]. It is thus most likely that they are manifestations of the same physical mechanism.

It is also interesting to compare the parameters of the static humps observed here, which form due to the attraction by the charged tip, with those of the multielectron dimples studied in [11], which result from a self-organized process. The relevant parameters are listed in Table II. The numbers in the table are very approximate, since both the humps and the dimples were observed in a certain range of conditions that influence their size. It is clear that the two types of deformations are quite

TABLE II. Parameters of the static humps and dimples at the free surface of liquid He observed in the present work and in [11].

	Hump (present work)	Dimple [11]
T (K)	2.1	2.5
Diameter FWHM (mm)	2.0	1.2
Height/depth (mm)	0.3	0.13
E (V/cm)	900	2900
Charge (C)	10^{-10}	10^{-12}

similar. The Taylor cones observed in the present experiment contain a significantly higher electric charge and therefore are larger than the dimples studied in [11], although the applied field strength is lower. It would be interesting to compare the Taylor cone and the dimple close to their respective breakdown thresholds, i.e., close to the emission of a jet and a multielectron bubble, respectively.

C. Trapped particles as dusty plasma

Some time ago it was proposed that an array of charged micro- or nanoparticles deposited above the free surface of superfluid He represents a perspective model system for studies of two-dimensional dusty plasmas [39]. It can be used to study the physics of strongly coupled Coulomb systems, including phase transitions, collective mode behavior, and transport properties under clean and well-controlled conditions. In the present experiment the particles are trapped underneath the liquid He surface, in close analogy with the proposal [39]. At present, our experimental technique does not allow us to control and adjust the size of the trapped particles. However, we have recently demonstrated [18,36] that observations of particle motion in the vertical direction allow one to infer their size distribution and the amount of charge attached to a single particle. In the future, it will be interesting to investigate the collective motion of particles trapped under the surface and compare it with the other known two-dimensional dusty plasma systems.

VI. CONCLUSIONS

In order to study the electrohydrodynamic behavior of charged liquid surfaces, superfluid helium is a unique system, because it is the cleanest dielectric liquid available and intrinsically does not contain any impurities or charged species. It thus provides an ideal testbed for investigating phenomena in which impurities are introduced artificially. In our work we have focused on the effect of charged particles accumulated underneath the free surface of liquid helium, after they had been generated in the bulk liquid by means of laser ablation from a metallic barium target. The particles collected at the surface exhibit a broad charge and size distribution, as evidenced by the spacing of the particles and the light scattered from them. For this heterogeneous system, the development of the Taylor cone in high external electric fields is found to be similar to that in charged homogeneous liquid surfaces, with respect to both the static deformation and the development of electrohydrodynamic instability and jet formation. A comparison with simulations allowed us to determine the charge density at the center of the Taylor cone, which goes up to some 10^{13} e/m². If a sizable fraction of these charges were in the form of Ba ions, we would be able to detect them spectroscopically. Yet in spite of the fact that such ions were observed in the bulk liquid, no signal from Ba⁺ ions at the surface could be detected. This negative result suggests that an agglomeration process was taking place at the surface, perhaps mediated by the presence of the nanoscopic and mesoscopic metal particles. Studies of Ba⁺ ions at a helium surface have thus failed so far, but it will be interesting to identify the origin of the loss of these ions. In addition, the system of

charged particles trapped at the helium surface lends itself to studies of two-dimensional dusty plasmas or to use as tracers for investigating flow phenomena like quantum turbulence at the surface of superfluids.

ACKNOWLEDGMENTS

P.M. would like to thank Frederic Aitken for the stimulating discussions. This work was supported by JSPS KAKENHI Grant No. JP24000007.

-
- [1] G. Taylor, *Proc. R. Soc. London A* **280**, 383 (1964).
 [2] G. I. Taylor and A. D. McEwan, *J. Fluid Mech.* **22**, 1 (1965).
 [3] R. T. Collins, J. J. Jones, M. T. Harris, and O. A. Basaran, *Nat. Phys.* **4**, 149 (2008).
 [4] A. L. Yarin, S. Koombhongse, and D. H. Reneker, *J. Appl. Phys.* **90**, 4836 (2001).
 [5] P. Kim, C. Duprat, S. S. H. Tsai, and H. A. Stone, *Phys. Rev. Lett.* **107**, 034502 (2011).
 [6] A. M. Ganan-Calvo, N. Rebollo-Munoz, and J. M. Montanero, *New J. Phys.* **15**, 033035 (2013).
 [7] E. O. Elele, Y. Shen, D. R. Pettit, and B. Khusid, *Phys. Rev. Lett.* **114**, 054501 (2015).
 [8] P. Leiderer, *J. Low Temp. Phys.* **87**, 247 (1992).
 [9] V. B. Shikin, *Phys. Usp.* **54**, 1203 (2011) [*Usp. Fiz. Nauk* **181**, 1241 (2011)].
 [10] M. W. Cole, *Rev. Mod. Phys.* **46**, 451 (1974).
 [11] P. Leiderer, W. Ebner, and V. B. Shikin, *Surf. Sci.* **113**, 405 (1982).
 [12] A. P. Volodin, M. S. Khaikin, and V. S. Edel'man, *JETP Lett.* **26**, 543 (1977) [*Pis'ma Zh. Eksp. Teor. Fiz.* **26**, 707 (1977)].
 [13] U. Albrecht and P. Leiderer, *Europhys. Lett.* **3**, 705 (1987).
 [14] V. Vadakkumbatt, E. Joseph, A. Pal, and A. Ghosh, *Nat. Commun.* **5**, 4571 (2014).
 [15] J. J. Niemela, *J. Low Temp. Phys.* **109**, 709 (1997).
 [16] A. P. Volodin and M. S. Khaikin, *JETP Lett.* **30**, 572 (1979) [*Pis'ma Zh. Eksp. Teor. Fiz.* **30**, 608 (1979)].
 [17] A. A. Levchenko, G. V. Kolmakov, L. P. Mezhev-Deglin, M. G. Mikhailov, and A. B. Trusov, *Low Temp. Phys.* **25**, 242 (1999) [*Fiz. Nizk. Temp.* **25**, 333 (1999)].
 [18] P. Moroshkin, R. Batulin, P. Leiderer, and K. Kono, *Phys. Chem. Chem. Phys.* **18**, 26444 (2016).
 [19] I. Baumann, M. Foerste, K. Layer, G. zu Putlitz, B. Tabbert, and C. Zühlke, *J. Low Temp. Phys.* **110**, 213 (1998).
 [20] Y. Moriwaki and N. Morita, *Eur. Phys. J. D* **13**, 11 (2001).
 [21] P. Moroshkin, V. Lebedev, and A. Weis, *Phys. Rev. Lett.* **102**, 115301 (2009).
 [22] R. Batulin, P. Moroshkin, D. Tayurskii, P. Blumhardt, P. Leiderer, and K. Kono, *J. Low Temp. Phys.* **175**, 63 (2014).
 [23] See Supplemental Material at <http://link.aps.org/supplemental/10.1103/PhysRevE.95.053110> for details.
 [24] H. J. Reyher, H. Bauer, C. Huber, R. Mayer, A. Schäfer, and A. Winnacker, *Phys. Lett. A* **115**, 238 (1986).
 [25] R. Batulin, P. Moroshkin, Y. Lysogorskiy, D. Tayurskii, and K. Kono (unpublished).
 [26] P. Moroshkin, V. Lebedev, B. Grobety, C. Neururer, E. B. Gordon, and A. Weis, *Europhys. Lett.* **90**, 34002 (2010).
 [27] E. B. Gordon, A. V. Karabulin, V. I. Matyushenko, V. D. Sizov, and I. I. Khodos, *Appl. Phys. Lett.* **101**, 052605 (2012).
 [28] L. F. Gomez, E. Loginov, and A. F. Vilesov, *Phys. Rev. Lett.* **108**, 155302 (2012).
 [29] E. Latimer, D. Spence, C. Feng, A. Boatwright, A. M. Ellis, and S. Yang, *Nano Lett.* **14**, 2902 (2014).
 [30] P. Thaler, A. Volk, F. Lackner, J. Steurer, D. Knez, W. Grogger, F. Hofer, and W. E. Ernst, *Phys. Rev. B* **90**, 155442 (2014).
 [31] A. Ramos and A. Castellanos, *Phys. Lett. A* **184**, 268 (1994).
 [32] H. Li, T. C. Halsey, and A. Lobkovsky, *Europhys. Lett.* **27**, 575 (1994).
 [33] W. Guo, D. Jin, G. M. Seidel, and H. J. Maris, *Phys. Rev. B* **79**, 054515 (2009).
 [34] A. L. Fetter, in *The Physics of Liquid and Solid Helium, Part I*, edited by K. H. Bennemann and J. B. Ketterson (Wiley, New York, 1976), pp. 207–305.
 [35] A. M. Ganan-Calvo, *Phys. Rev. Lett.* **79**, 217 (1997).
 [36] P. Moroshkin, P. Leiderer, and K. Kono, *Phys. Fluids* **29**, 047106 (2017).
 [37] K. W. Schwarz, *Phys. Rev. A* **6**, 837 (1972).
 [38] M. Foerste, H. Guenther, O. Riediger, J. Wiebe, and G. zu Putlitz, *J. Low Temp. Phys.* **110**, 231 (1998).
 [39] M. Rosenberg and G. J. Kalman, *Europhys. Lett.* **75**, 894 (2006).